J. Fluid Mech. (1977), *vol.* 81, *part* 3, *pp.* 439–464
Printed in Great Britain

Structure of the turbulent boundary in drag-reducing pipe flow

By B. U. ACHIA† AND D. W. THOMPSON
Department of Chemical Engineering, University of British Columbia, Vancouver V6T 1W5, Canada

(Received 5 January 1976)

The effect of a drag-reducing additive on the structure of wall turbulence in pipe flow was investigated experimentally. Real-time hologram interferometry was used for flow visualization and turbulence measurements. The real-time modulation of interference fringes by a refractive-index enhancer infused into the near-wall flow was recorded by medium-speed motion photography. The spanwise direction and the direction normal to the wall were studied to investigate the 'streaks' and 'bursts' that originate in the sublayer. A region of the flow was sampled for spatial and temporal correlations of concentration fluctuations to detect the scales of eddy interaction.

The addition of 50 p.p.m. by weight of Separan AP30 to water significantly altered the Newtonian wall-flow structure. The drag-reducing additive suppressed the formation of streaks and the eruption of bursts. When compared at the same wall shear, the sublayer period increased over the Newtonian value by a factor almost equal to the ratio of the corresponding non-dimensional streak spacings.

These results suggest a stabilized wall layer in the drag-reducing solution as compared with that of the Newtonian solvent, resulting in less turbulence production and reduced frictional drag. The role of the extensional viscosity of the dilute polymer solution is discussed as a possible mechanism for explaining the visualized and measured phenomena.

1. Introduction

The phenomenon of frictional drag reduction in turbulent fluid flow due to the addition of very small quantities of long-chain polymers has received considerable attention in recent years (e.g. Hoyt 1972). While the mechanism by which drag reduction occurs is still a debated topic it is widely accepted that the interaction of the turbulently flowing solution with the boundary region plays a major role. Wells & Spangler (1967) demonstrated this wall effect by injecting small amounts of polymer solution into different regions of a pipe flow. Wall injection produced immediate drag reduction while with centre-line injection drag reduction was delayed until the solution had diffused to the wall.

This finding has an important implication in the light of research on Newtonian boundary layers in the past decade (e.g. Kline *et al.* 1967; Corino & Brodkey 1969; Kim, Kline & Reynolds 1971). These workers have shown that turbulent fluid motion

† Present address: Imperial Oil Enterprises Ltd, Research Department, Box 3022, Sarnia, Ontario N7T 7M1, Canada.

in the near-wall layer has a characteristic spatial structure made up of 'streaks' and 'bursts'. The periodic ejection of fluid bursts from the wall layer and their interaction with the outer flow are believed to be major factors in the generation and maintenance of turbulence. A proposed model is discussed by Offen & Kline (1975).

The wall-layer streaks observed by Kline *et al.* (1967) are believed to result from the inflow–outflow fluid motion caused by streamwise counter-rotating 'Townsend' eddies. The resulting vortex compression and stretching at the wall lead to a secondary streamwise vorticity and to the growth of sublayer instability. This instability, in the presence of a temporary adverse pressure gradient caused by upstream-generated spanwise vortices sweeping the wall layer, leads to ejections of fluid from the wall layer into the mean flow.

Gadd (1965) suggested that the damping of turbulence by polymer additives could result from a reduction in bursting. The damping effect was attributed to a polymer solution's high resistance to elongational strain, whereby vortex stretching motions during streak formation and bursting are suppressed. The analysis of Lumley (1973) of an isolated molecule in pure strain indicates that molecular expansion takes place and that very dilute polymer solutions may undergo an effective change in viscosity when subjected to elongational strain. While there is no direct evidence of this in infinitely dilute solutions, the measurements of Metzner & Metzner (1970) and Oliver & Bragg (1973) with relatively dilute polymer solutions have demonstrated the extensional-viscosity effect.

Studies of the structure of the near-wall flow during drag-reduction have been limited owing to serious difficulties in the use of conventional probes and flow-visualization techniques with dilute polymer solutions. Novel techniques adapted to overcome the uncertainties of conventional schemes include the use of air-bubble and particle streak photography (Seyer & Metzner 1969; Rollin 1971; Carpenter 1973), laser-Doppler anemometry (Rudd 1972), wall-embedded electrochemical probes (Fortuna & Hanratty, 1972), photochromic dye tracers (Arunachalam, Hummel & Smith 1972) and wall-layer dye injection (Donohue, Tiederman & Reischman 1972). These studies have shown that the wall-layer turbulence structure during drag-reducing flow is substantially modified relative to the case of Newtonian flow, the most notable feature being the reduction in bursting.

This paper describes the results of measurements of near-wall flow structure by an interferometric flow-visualization technique. The results are interpreted in the light of a drag-reduction mechanism based on the polymer solution's high resistance to stretching motions.

2. Visualization of drag-reducing flows

The ability of visualization techniques to provide detail of an area of the flow field, rather than point data as probes do, has been illustrated by numerous studies in the literature. This study was specifically aimed at obtaining pictures of the wall region during drag reduction. Further, data were required that could be objectively and quantitatively analysed and that had sufficient resolution to display the fine-grained features of the flow.

The requirements for the visualization of drag-reducing flow are somewhat stricter than those for Newtonian flow. The basic rule for flow visualization is to make the

physical structures as large as possible and the fluctuations in time as small as possible. A low wall shear velocity u_*, generally less than 1 cm/s, is desirable to keep the fluctuation frequencies small. The restrictions posed by drag-reducing flow are threefold.

(i) Drag reduction in pipes is not usually observed below a threshold wall shear, thus requiring experiments to be done at values higher than the onset wall shear.

(ii) Drag-reducing flows are diameter sensitive. As a result, large ducts do not produce as much drag reduction as would a pipe of small diameter with the same polymer solution.

(iii) The solution viscosity increases rapidly with polymer concentration. In order to make comparisons with the Newtonian solvent, it is most desirable to keep the solution viscosity as close as possible to that of the solvent.

These restrictions limit the flow-visualization experiment to flow cross-sections of relatively small effective diameter and to low polymer cncentrations (3–10 cm and 25–150 p.p.m. by weight respectively). The useful Reynolds-number range, with a good drag-reducing polymer, would then be about 10000–20000, providing drag reductions of up to 60 %.

For this study, a 2·63 cm I.D. pipe was chosen with a flow Reynolds-number range of 6000–15000. Owing to the small dimension of this pipe the available flow-visualization schemes were further restricted. In order to observe 'streak' and 'burst' structures at the wall, a continuous tagging of the fluid with real-time recording was essential. This necessity ruled out intermittent methods like streak photography. While the hydrogen-bubble time-line technique was a prime candidate, the physical difficulty in locating a bubble wire at the pipe wall and ensuring its satisfactory operation made it unsuitable. Further, it has been shown recently (Donohue 1973) that polymer additives may adversely affect the shedding of hydrogen bubbles from wires.

While wall dye injection is quite simple to perform, it does not provide a quantitative sampling scheme and has poor resolution as the physical scales become small. To improve resolution and to provide a means of quantitative analysis, the refractive index of the wall layer was enhanced and flow patterns studied by interferometry. However, since conventional interferometry is limited to test sections with optically flat and parallel windows, a hologram-interferometric technique was used (Achia & Thompson 1972).

3. Experimental apparatus and procedure

3.1. *The flow-visualization apparatus*

The blow-down pipe flow apparatus shown in figure 1 was used to obtain gross flow data and to conduct interferometric visualization studies. A detailed description of the flow apparatus and hologram-interferometer may be found in Achia (1975).

Distilled water was used for the Newtonian flow tests. A solution of Separan AP30 (a Dow Chemical Co. poly-acrylamide) of concentration 50 p.p.m. by weight in distilled water was used in the drag-reducing tests. The viscosity of the solution was 1·443 cP as measured with a Cannon-Fenske viscosimeter.

The flow patterns in the wall region were made visible by infusing a refractive-index enhancer into the flow. This enhancer was a 3·5 % by volume solution of propylene glycol. The solution was made up both in water and in the drag-reducing fluid for use in

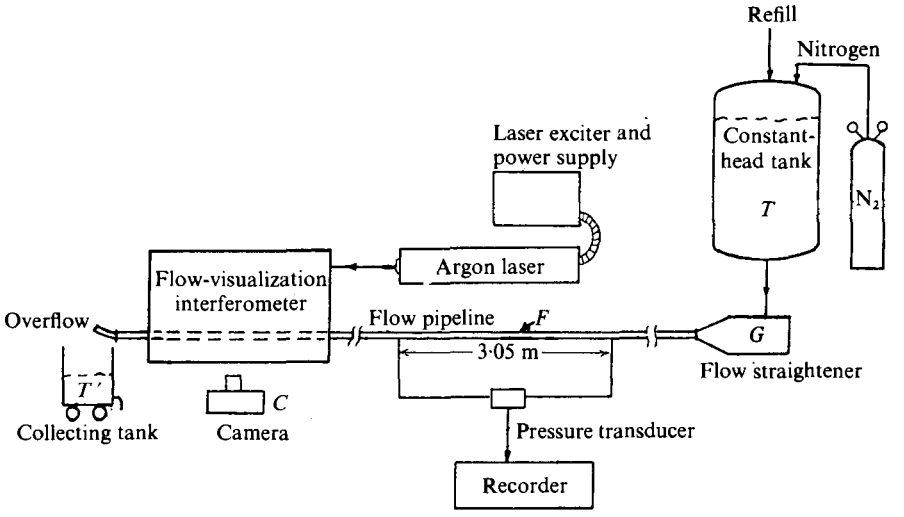

FIGURE 1. The flow-visualization apparatus.

their respective flows. The choice of the enhancer was governed by the following requirements.

(*a*) It would neither affect the physical properties (ρ, ν) of the distilled water or Separan solution, nor react chemically with them when introduced into the flow.

(*b*) A very small amount of the enhancer would produce a large change in refractive index. Typically, the infusion rate was about 0·02 ml/s at a Reynolds number of about 10000 ($Q \simeq 225$ ml/s).

Phase variations in the flowing stream due to the enhancer introduced upstream of the observation field were visualized and recorded as real-time distortions of an interference fringe system. These fringe movements provided information on turbulence in the wall layer (detailed in §4.2).

3.2. *Wall-layer co-ordinates*

The test section consisted of a region of the pipe wall 6–8 cm in length. To observe both the spanwise direction and the direction normal to the wall, two separate views were necessary. Figure 2 shows the geometry of the spanwise view used to observe the streaky structure. Since the spanwise and normal views are mutually perpendicular, the co-ordinate axes as projected onto the hologram plane H are rotated through 90° between the views. The co-ordinate system was so chosen that in each of the views the x axis is parallel to and in the direction of the mean flow (the streamwise direction), the y axis is normal to the pipe wall and the z axis is along the pipe wall, perpendicular to the flow and the hologram plane (the spanwise direction).

The inset in figure 2 shows the cross-section of the flow test section. This portion of the pipe, about 50 cm in length, was fabricated from a 5 cm square Plexiglas block in 12 cm lengths which were carefully aligned. The circular pipe section had a flat wall (exaggerated in figure 2) which formed the region for flow studies. This shape of test section was used since in a fully circular pipe light refraction does not permit an edge view *at* the wall. This flattening of the pipe wall affected the bulk flow rate by about 1 % and no secondary flows were induced since the change in shape was very gradual. A wall slot

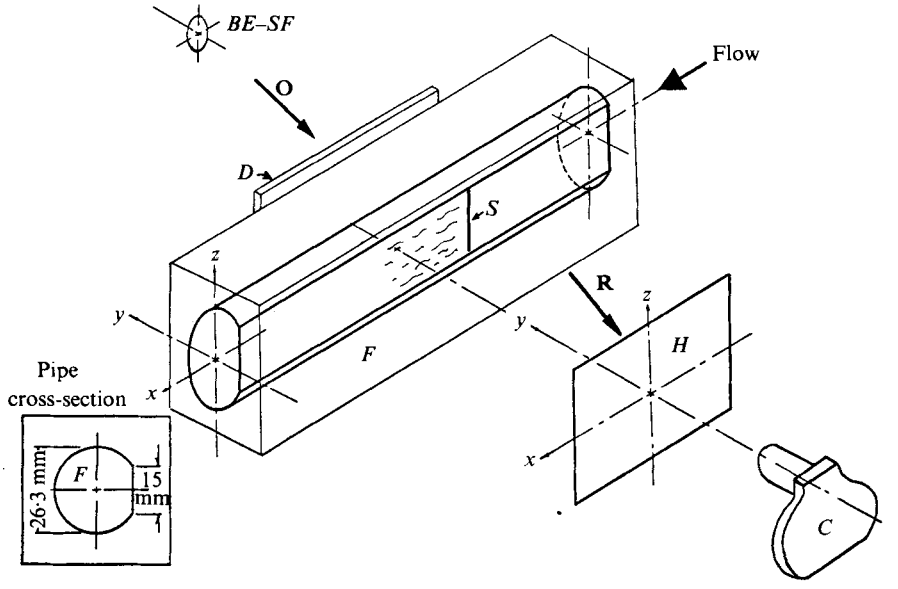

FIGURE 2. Plan view of the pipe wall and the co-ordinate axes. *C*, camera; *D*, diffuser; *F*, test section; *S*, wall slot; *BE–SF*, beam expander and spatial filter; *H*, hologram; **O**, object beam; **R**, reference beam.

S, 0·2 × 14 mm, was located in the flat wall for infusion of the refractive-index enhancer. Visualization studies were made in the region up to 7 cm downstream of the slot. Details of the fabrication of the pipe test section, the refractive-index enhancement and the preparation and characterization of the polymer solution may be found in Achia (1975).

3.3. *Experimental procedure*

The initial condition was recorded on the hologram with the entire pipeline filled with the test liquid (distilled water or Separan solution). A fringe pattern of the desired orientation and frequency was adjusted by controlled displacement of the processed hologram, which was mounted on micrometer-operated tables (Achia 1972).

The real-time fringe display during flow experiments was recorded on 16 mm film at frame rates of between 32 and 200 frames/s using the movie camera *C* (Red Lake Laboratories Hycam or Bolex H16). High-speed films, Kodak 2485 and Kodak 4XN, were used.

4. Measured quantities and data analysis

4.1. *Gross flow quantities*

The basic quantities measured were the flow rate Q and the corresponding pressure drop ΔP. The Reynolds number Re was based on the pipe diameter D, the mean flow velocity $\overline{U}$ and the solution's kinematic viscosity ν. The Fanning friction factor f is given by

$$\tfrac{1}{2}f = \langle \tau_W \rangle / \rho \overline{U}^2, \tag{1}$$

where the mean wall shear stress $\langle \tau_W \rangle = D\Delta P/4L$ dynes/cm^2. The wall shear velocity

$$u_* = (\langle \tau_W \rangle / \rho)^{\frac{1}{2}} \text{ cm/s}. \tag{2}$$

The percentage drag reduction at a given Q is defined as

$$DR = \left| \frac{\Delta P_N - \Delta P_{DR}}{\Delta P_N} \right|_Q \times 100\,\%. \tag{3}$$

These quantities were used to characterize the flows in which the wall turbulence was studied in greater detail by visualization.

4.2. *Interpretation of the fringe field*

Reduction of interferometric data to obtain information on the flow structure in the wall layer is based on the solution of the integral for the phase S of the light wave:

$$S(x,z) = \frac{k}{\lambda_l} \int \Delta n \, dy, \tag{4}$$

where k is an optical constant characteristic of the medium traversed by the beam, λ_l is the wavelength of the laser light source, Δn is the change in refractive index causing the phase change in the beam and the integration path is the beam path. The coordinate axes referred to in this equation are shown in figure 2. In this flow situation, the concentration distribution of the enhancer is confined to a very thin layer adjacent to the wall, essentially the region $y^+ \equiv yu_*/\nu < 10$. The sampling region is immediately downstream of the infusion slot, so that the enhancer has not had sufficient time to diffuse far in the normal (y) direction. It is then reasonable to assume that the refractive index n varies only in the wall layer, for which $y^+ < 10$, so (4) can be simplified to give

$$S(x,z) = (k/\lambda_l)\, y[n_r(x,z) - n_t(x,z)]. \tag{5}$$

In (5), n_r and n_t are the refractive indices under reference and test conditions respectively.

The interferogram is interpreted as a distribution of phase difference $S(x,z)$ or analogously as a distribution of refractive index $n(x,z)$ according to (5). The concentration distribution, which is the quantity of interest, can be determined from

$$\Delta C(x,z) = \lambda_l \frac{1}{ky} \frac{dC}{dn} S(x,z) \tag{6}$$

or expressed as the concentration difference per interference fringe $\Delta C/\Delta S$. For the propylene glycol solution used in this study the refractive index varied linearly with concentration within the measuring range, so that the concentration field was directly proportional to the fringe shift. Hence discussions of the turbulent concentration field in terms of either C or S are equivalent. Since the measurement of enhancer concentration in the flow required calibration, it was convenient to measure and express all fluctuations in terms of the fringe shift, one fringe width d being the distance between two adjacent bright or dark bands.

4.3. *Method of fringe read-out*

The varying concentration field in the wall layer, the fluctuation of which is related to the turbulent flow field, was analysed statistically. The instantaneous concentration C can be regarded as

$$C = \bar{C} + c, \tag{7}$$

where $\bar{C}$ is the mean concentration and c is the fluctuation in concentration about the mean.

Experimentally, the space-average fringe shift $\bar{S}_z$ along a selected line in the z direction was determined from each of a set of interferograms of the flow taken at different instants in time. This set of space-averaged fringe shifts was averaged to give a mean space average $\bar{S}$.

The space-average fringe shift at any instant t is defined as

$$\bar{S}_z = \frac{1}{N} \sum_{i=1}^{N} S(z_i) \tag{8}$$

at a fixed value of x. Sampling this over a number of frames at different times gives

$$\bar{S} = \frac{1}{T} \sum_{t=1}^{T} \bar{S}_z. \tag{9}$$

The sampling line at A in figure 3 (b) (plate 1) was divided into a number of segments of width Δz in the spanwise direction so as to resolve the streak spacing. The choice of Δz was limited by the resolution length of the interferogram, which is typically about one-eighth of the fringe spacing d. In this work, 24 segments were used in the 14 mm span of the wall, giving $\Delta z = 0{\cdot}583$ mm. With the value $d \cong 3$ mm that was generally used, the minimum resolution was about 0·38 mm.

Measured fringe shifts were used to compute certain spatial and temporal turbulence parameters that describe the flow in the wall region. Details of fringe measurements, computer programs and data analysis are given in Achia (1975).

4.4. *Wall-layer turbulence parameters*

Determination of streak spacing λ from the spatial correlation of concentration $R_c(\xi)$. This method of objective determination of the streak spacing λ using a spatial correlation coefficient is analogous to the work of Schraub & Kline (1965). They used hydrogen-bubble time-line traces of velocity to determine the spatial structure. In this work, an instantaneous spanwise concentration profile obtained from an interference fringe was used.

The spanwise correlation of concentration $R_c(\xi)$ is defined as

$$R_c(x_0, y_0, \Delta z; t_0) = \frac{\int c(z)\, c(z+\Delta z)\, dz}{[\int c(z)^2 c(z+\Delta z)^2\, dz]^{\frac{1}{2}}}. \tag{10}$$

From the experimental data, it is easier to express $R_c(\xi)$ in terms of the fringe shift S than in terms of concentration. Hence (10) can be modified to

$$R_c(x_0, y_0, j\Delta z; t_0) \equiv \frac{\frac{1}{N} \sum_{i=1}^{N} [S(z_i) - \bar{S}]\, [S(z_i + j\Delta z) - \bar{S}]}{\left\{ \frac{1}{N} \sum_{i=1}^{N} [S(z_i) - \bar{S}]^2 \frac{1}{N} \sum_{i=1}^{N} [S(z_i + j\Delta z) - \bar{S}]^2 \right\}^{\frac{1}{2}}}, \tag{11}$$

where the spatial separation $\xi \equiv \Delta z$.

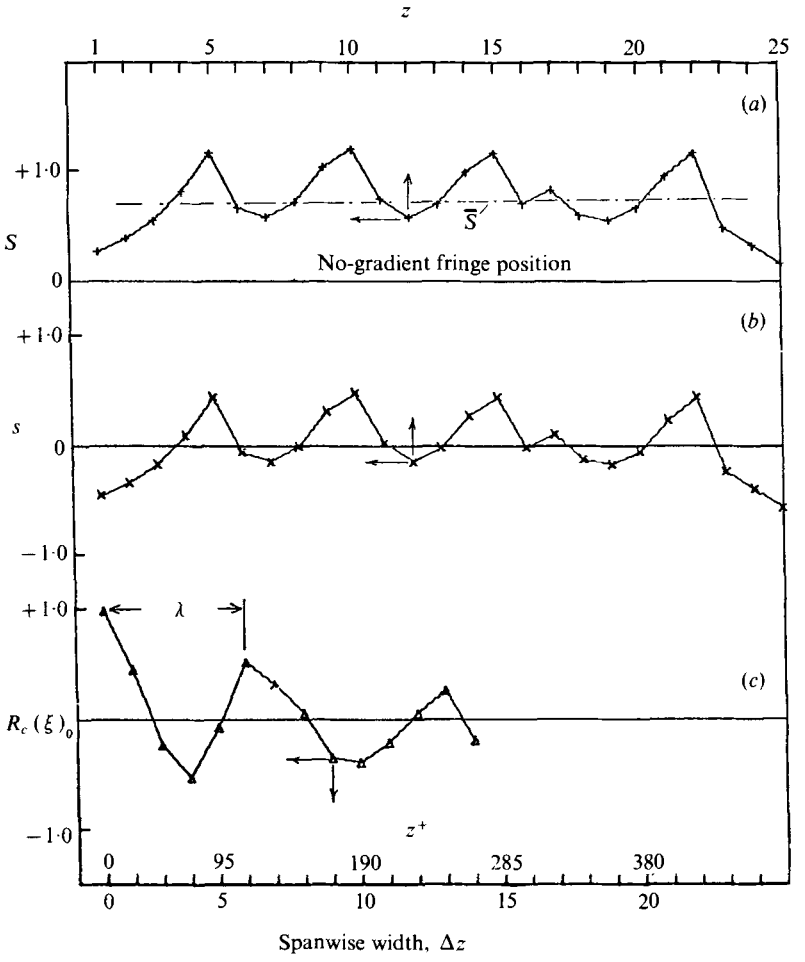

FIGURE 4. Analysis of a typical interferogram for streak spacing λ. (*a*) Instantaneous fringe shift S. (*b*) Fluctuation s about the mean. (*c*) Spatial correlation coefficient $R_c(\xi)$. (The z^+ scale is for run *W3s*; $u_* = 3{\cdot}25$ cm/s, $\Delta z = 0{\cdot}583$ mm.)

$R_c(\xi)$ provides information on the spatial structure of the flow. A definable spatial structure can be considered to exist when the turbulent concentration over the spanwise field is correlated. Thus, at separation distances where the correlation is non-zero, the behaviour of $R_c(\xi)$ provides information on the spatial scales. The simplest interpretation is that the distance between the origin and the first positive peak in $R_c(\xi)$ can be taken as a measure of the spatial scale λ of the wall-layer streaks.

The analysis performed to determine the streak spacing in a typical flow interferogram, of the kind shown in figure 3 (*b*), is described in figure 4. The analysis uses fringe-shift measurements at a station A located downstream of the wall slot. This location represents $x = 0$, the lower edge of the frame denoting $z = 1$. The instantaneous fringe shift, read from a frame of the movie film using a microdensitometer, is shown in figure 4 (*a*). The baseline of this trace corresponds to the fringe position in flow with no refractive-index gradients. Figure 4 (*b*) shows the fluctuation about the mean fringe shift. The spanwise spatial correlation coefficient $R_c(\xi)$ for this frame is shown in figure

4(*c*). The distance from the origin to the first positive peak of the correlation function for each frame gives a measure of the streak spacing λ for that frame.

$R_c(\xi)$ was computed for a number of frames of plan-view interferograms (40–50) sampled at random. The time interval between two samples was kept long enough so that they were not correlated in time. A histogram of peak positions was used to obtain the mean λ for each flow condition.

Determination of sublayer period T_S from the autocorrelation of concentration $R_c(\tau)$. In a similar manner to the spatial correlation, the autocorrelation can provide information on the time scale of the wall-layer structure. The autocorrelation at a single point in the flow field over a period of time may be expressed in terms of the fringe shift as

$$R_c(x_0, y_0, z_0; j\Delta t) \equiv \frac{\frac{1}{N}\sum_{i=1}^{N}[S(t_i)-\bar{S}]\,[S(t_i+j\Delta t)-\bar{S}]}{\left\{\frac{1}{N}\sum_{i=1}^{N}[S(t_i)-\bar{S}]^2\,\frac{1}{N}\sum_{i=1}^{N}[S(t_i+j\Delta t)-\bar{S}]^2\right\}^{\frac{1}{2}}}, \tag{12}$$

where the time lag $\tau \equiv \Delta t$ and

$$\bar{S} = \frac{1}{N}\sum_{i=1}^{N} S(t_i). \tag{13}$$

The distance between peaks in time units of an autocorrelation trace may be interpreted as the mean period of the signal being correlated. In the absence of a large number of cycles, the distance from the origin to the first rerise positive maximum of the $R_c(\tau)$ curve is taken as an estimate of the mean period T_S. $R_c(\tau)$ was computed from fringe-shift measurements taken from a string of sequential motion-picture frames. The length of the sampling period was 20 s, i.e. 40 times the maximum lag time $\tau_{\max} \simeq 0{\cdot}5$ s of the autocorrelation.

Intensity of turbulent concentration fluctuation. The relative intensity I_c of the turbulent concentration fluctuation is defined as

$$I_c \equiv \frac{\{\overline{(c^2)}\}^{\frac{1}{2}}}{\bar{C}} = \frac{\left\{\frac{1}{N}\sum_{i=1}^{N}[S(z_i)-\bar{S}]^2\right\}^{\frac{1}{2}}}{\bar{S}}. \tag{14}$$

The mean I_c was measured for each of the individual frames (40–50) that were used to obtain spatial correlations. From these samples of I_c data, the means for each of the runs were obtained.

The burst rate F and burst time interval T_B. The edge-view motion pictures were used to determine the rate of bursting in water and Separan solutions. The fluid with enhanced refractive index is seen to move away from the wall in intermittent bursts. These bursts carry distinguishable filaments of fluid from the wall layer into the bulk of the flow.

Bursts occurring in a region 14 mm in spanwise width and 6 cm in the flow direction were counted during a period of 30–60 s. The motion pictures were run both frame-by-frame and in slow motion. Running the film in reverse was often helpful in identifying bursts more clearly: in this way, ejected filaments would come together and collapse at the wall. This method of burst visualization using dye is detailed in Kline *et al.* (1967).

F has the units of bursts $\times$ s^{-1} cm^{-1}. T_B, a quantity computed using values of the bursting rate F and streak spacing λ, is given by the equation

$$T_B = (F\lambda)^{-1} \text{ s/burst}. \tag{15}$$

This relationship for T_B was suggested by Kim *et al.* (1971) on the basis of their experimental findings and those of Schraub & Kline (1965) for zero-pressure-gradient Newtonian flows over a wall of a rectangular channel.

5. Experimental results

Six flows were selected for detailed visualization studies: three with water (Newtonian) and three with drag-reducing 50 p.p.m. by weight Separan AP30 solutions (see table 1). Each run consisted of two parts: a wall plan view to study streaks and a wall edge view to observe bursts. Gross flow measurements were made first, followed by measurements of turbulence structure and visual observations of the flow in the near-wall layer. For the latter, representative visual impressions are provided wherever possible as still pictures. However, since the turbulence being observed changes with time and space, a true and complete impression can be obtained only from motion pictures. A display movie has been prepared for this purpose (Achia & Thompson 1974).

5.1. *Gross flow measurements*

Gross flow tests were conducted first to establish the drag-reducing characteristics of Separan AP30–water solutions of various concentrations: 0, 25, 50, 100 and 150 p.p.m. by weight. The distilled-water data served as a check on the flow apparatus and were found to agree with the Newtonian turbulent–smooth line given by the equation

$$f = 0{\cdot}046\, Re^{-0{\cdot}20}. \tag{16}$$

All the gross-flow measurements are shown on the plot of Fanning friction factor *vs.* Reynolds number in figure 5. The Reynolds number for Separan is based on the solution viscosity that was determined using a Cannon-Fenske viscosimeter.

Figure 5 reveals the regimes of drag-reducing flow exhibited by the Separan solutions. The 'onset' of drag reduction, which may be estimated roughly for each solution as the intersection of the extrapolated solution lines with the Newtonian turbulent–smooth line, is strongly concentration dependent. So also is the percentage of drag reduction at a given Reynolds number. In order to select a solution for more detailed visualization studies, the criteria detailed in § 2, i.e. the requirements for flow visualization, were applied. The 50 p.p.m. by weight Separan solution, while having a viscosity of 1·443 cP, could provide good drag reduction in the Reynolds number range 6000–15000. The drag-reduction visualization runs had an onset friction velocity of $u_* = 1{\cdot}7$ cm/s.

5.2. *Visualization studies*

The streaky structure at the wall. Figure 3 (plate 1) shows the characteristic wall-layer streaks as visualized with both dye infusion and fringe patterns for an enhanced refractive index. These dye tests were done to check the observations of workers who have reported streak and burst formation at the wall during turbulent flow in large channels (e.g. Kline *et al.* 1967; Donohue *et al.* 1972). Figure 3 (*a*) shows the characteristic streaky structure when the flow is turbulent. In laminar flow, the dye was seen to

Fluid	Run	Reynolds number Re	Friction factor f	Flow rate Q (ml/s)	Bulk velocity $\bar{U}$ (cm/s)	Pressure drop ΔP (cm H_2O per 305 cm of pipe)	Shear velocity u_* (cm/s)	Drag reduction (%)
Water (distilled)	$W1$	6550	0·00745	135·0	24·9	1·10	1·52	0
$\nu = 0{\cdot}0100$ cm²/s	$W2$	10900	0·00695	225·0	41·5	2·85	2·45	0
	$W3$	14500	0·00672	300·0	55·3	6·15	3·25	0
Separan AP30	$S1$	7400	0·00574	220·0	40·5	2·25	2·18	20
50 p.p.m. by weight	$S2$	9750	0·00455	290·0	53·4	3·10	2·56	32
(in distilled water),	$S3$	14800	0·00360	440·0	81·1	5·65	3·45	44
$\nu = 0{\cdot}0144$ cm²/s								

TABLE 1. Summary of flow conditions for holographic visualization runs.

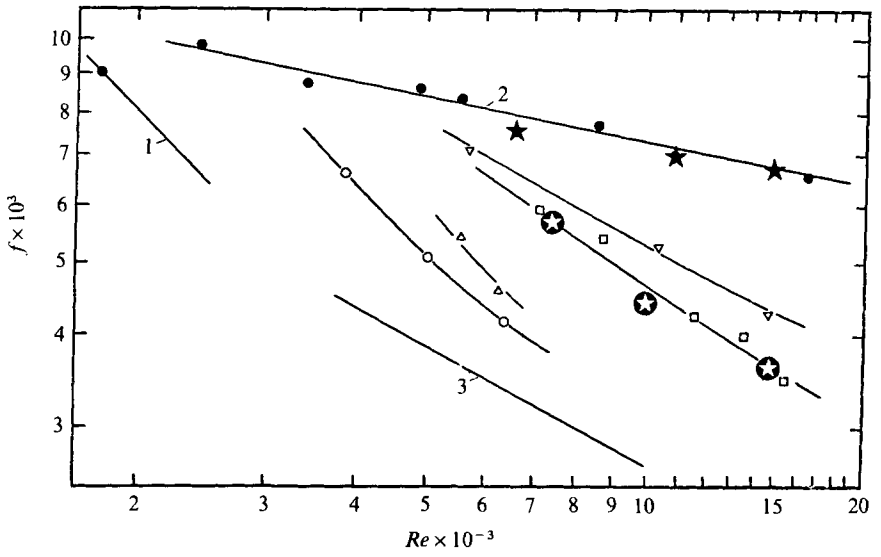

FIGURE 5. Fanning fraction factor *vs.* Reynolds number for gross flow of solutions of Separan AP30 in distilled water in a smooth 2·63 cm pipe. 1, laminar line; 2, Newtonian turbulent–smooth line; 3, drag-reduction asymptote; ★, ✪, visualization runs. Separan concentration (p.p.m. by weight); ●, 0; ▽, 25; □, 50; △, 100; ○, 150.

leave the wall slot in the form of a uniform sheet. The dye tests further showed that the design of the flow cross-section was satisfactory. There were no observable corner effects at the points where the pipe's circular section was flattened (see inset in figure 2). When observed for a length of time, the streaks did not appear to form at specific locations on the pipe wall or at the infusion slot.

The results of the streak-spacing measurements in Separan and water are summarized in table 2. The physical streak spacing λ decreased with an increase in u_*. However, the non-dimensional streak spacing λ^+ appears to have a constant value for the water flows (see table 2 and figure 6).

While the three water flows have an almost constant non-dimensional streak spacing λ^+, the polymer solution shows an increase in λ^+ with increasing wall shear. The physical spacing λ in water becomes smaller with increasing u_*, while the reverse happens in the drag reducer. All these trends are shown in figure 6.

The limits of the increasing trend of λ and λ^+ in the drag-reducing Separan solution are not known. The data show that the rate of increase of λ decreases with increasing wall shear, while λ^+ increases almost linearly. The limiting maximum values of λ and λ^+ are not available from these experiments, which are limited by the flow-visualization considerations outlined in §2. In water, the rate of increase of λ decreases with increasing wall shear. The result is an almost constant mean λ^+ of 87.

The physical changes that occur in the near-wall flow owing to the addition of the drag reducer are rather dramatic when viewed in the motion pictures (Achia & Thompson 1974). Figure 7 (plate 2) compares Separan and water flow patterns at almost the same u_*: runs *S*3*s* and *W*3*s* in table 2. Frames 1*A* and 2*A* are no-gradient fringe patterns while frames 1*B–E* and 2*B–E* are gradient-enhanced flow patterns. The numbers seen on the Separan frames mark time elapsed from the start of filming; the

Fluid	Run	Drag reduction (%)	Shear velocity u_* (cm/s)	Physical streak spacing λ (cm)	Non-dimensional streak spacing λ^+	Relative intensity I_c
Water (Newtonian)	*W1s*	0	1·52	0·58	88	0·428
	W2s	0	2·45	0·32	79	0·429
	W3s	0	3·25	0·29	93	0·432
Separan AP30 solution (drag reducer)	*S1s*	20	2·18	0·75	114	0·404
	S2s	32	2·56	0·96	170	0·400
	S3s	44	3·45	0·98	235	0·362

TABLE 2. Low-speed streak-spacing data for water and 50 p.p.m. by weight Separan AP30 solution in pipe flow.

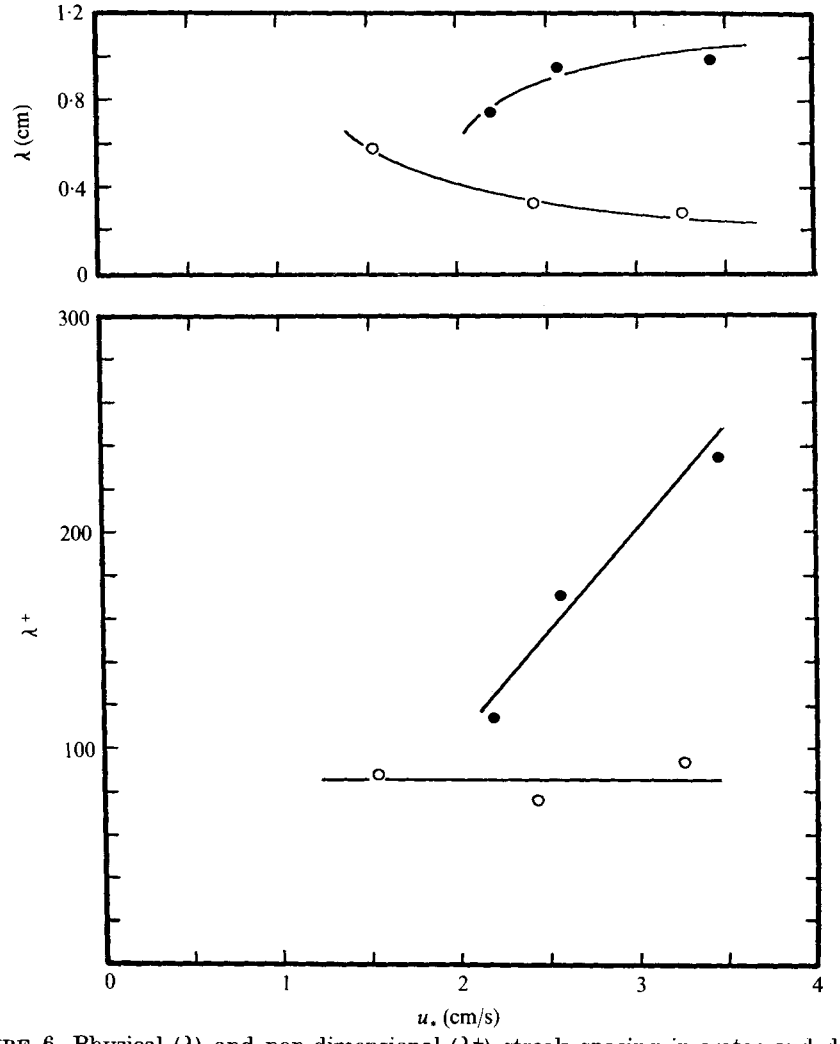

FIGURE 6. Physical (λ) and non-dimensional (λ^+) streak spacing in water and drag-reducing Separan AP30 solution. ○, water; ●, Separan.

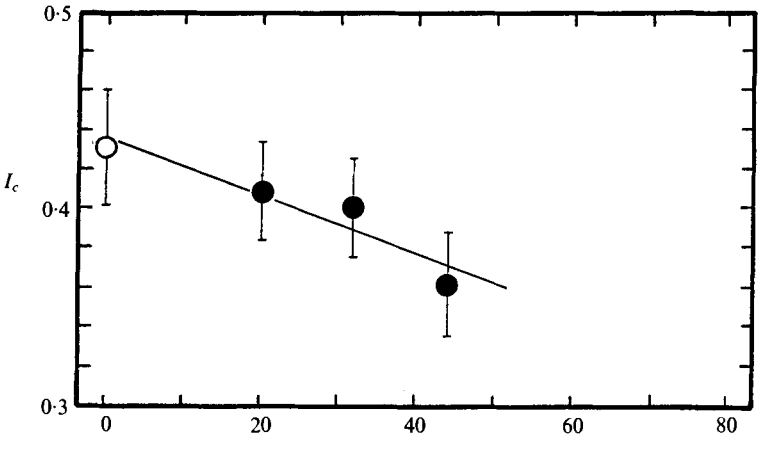

FIGURE 8. The effect of drag reduction on the relative intensity of the spanwise concentration fluctuation. ○ water; ●, Separan. $I_c = (\overline{c^2})^{\frac{1}{2}}/\overline{C}$.

water-flow frames were selected to correspond approximately in time to those for Separan.

A noticeable effect of the drag reducer on the near-wall flow structure is an increase in the spanwise scale of the 'saw-tooth' like concentration distribution compared with that for the water flow (compare frames 1*B–D* and 2*B–D*). Frames 1*C* and *D*, when compared with frames 2*C* and *D*, show that the structure in Separan persists over a longer time span. This persistence is easier to see in the motion picture.

The wall-layer flows of water and Separan are different whether compared at the same Reynolds number, the same mass flow rate or the same wall shear velocity. The characteristic increase in λ and the greater streak persistence in the drag reducer were noticeable at all times. In addition, the longitudinal extent of streaks was greater in the Separan solution and the spanwise 'flag-like' waving of the streaks was markedly reduced from that in water. Occasionally, in individual movie frames, the Separan flow appears to be similar to the water flow as in frames 1*E* and 2*E* of figure 7. This occurrence was relatively rare and became even less frequent with an increase in the flow rate.

The effect of drag reduction on the relative intensity I_c of the spanwise concentration fluctuation is shown in figure 8. Each point on figure 8 represents a mean I_c value from a sample of 40–50 flow interferograms taken at that flow condition. The visual observations are quantified as a small but definite reduction of I_c with reduced drag. I_c ranges from 0·36 to 0·40 in the flows of drag-reducing solution and is about 0·43 in the water flows. The small percentage reduction in I_c is not comparable to the large percentages of drag reduction (15 % *vs.* 40 % for *S*3).

The nature of bursting. Bursting refers to the sequence of events involved in the ejection of refractive-index-enhanced fluid from the wall layer into the bulk flow. The data on bursting are detailed in table 3. A description of the fluid's physical structure during bursting is made difficult by the rather large variations in the size and intensity of individual bursts and the chaotic motions associated with the bursting process. A description of the general characteristics is attempted with the aid of frames from the

Fluid	Run	Drag reduction (%)	Shear velocity u_* (cm/s)	Burst rate F (bursts/cm s)	Time between bursts, T_B (s/burst)	Non-dimensional burst time $T^+ = T_B u_*^2/\nu$	Streak lifetime T_S (s) from $R_c(\tau)$
Water (Newtonian)	*W1b*	0	1·52	4·2	0·41	95	0·300
$\nu = 0{\cdot}010$ cm²/s	*W2b*	0	2·45	22	0·14	84	0·098
	W3b	0	3·25	45	0·077	81	0·128
Separan AP30	*S1b*	20	2·18	10	0·13	43	0·313
50 p.p.m. by weight solution	*S2b*	32	2·56	5·1	0·21	96	0·285
(drag reducer)	*S3b*	44	3·45	18	0·057	47	0·255
$\nu = 0{\cdot}014$ cm²/s							

TABLE 3. Burst period T_B and streak lifetime T_S for water and 50 p.p.m. by weight Separan AP30 solution in pipe flow.

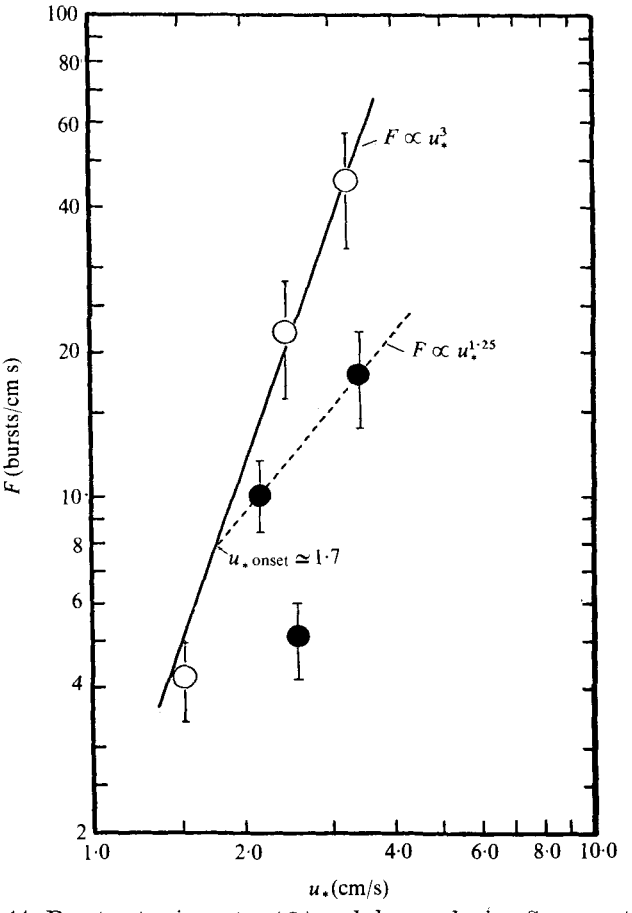

FIGURE 11. Burst rates in water (○) and drag-reducing Separan (●) flows.

motion pictures and simplified sketches, as shown in figure 9 (plate 3). The three stages of bursting, broadly classified as (i) streak lift-up, (ii) oscillatory motion and (iii) breakup by Kline *et al.* (1967), are retained to ease this description. There is no sharp demarcation between these three stages.

A series of consecutive frames of bursting in a water flow at $u_* = 2{\cdot}45$ cm/s is shown in figure 9. The undisturbed fringe pattern is shown in frame 0. In this picture, a low-speed streak is just lifting off from the pipe wall. The arrows in the subsequent pictures and the corresponding sketches point to a discrete fluid element as it moves downstream with the flow and outwards from the wall. A fluid burst is seen in frame 1 and further amplification of that burst is seen in frames 2 and 3. The wall-normal extent of the burst is seen to have grown rapidly from the near-wall region to $y^+ \simeq 150$ in a very short stream-wise distance. The breakup of the lifted-up fluid element is under way in frame 4. Frame 5 shows the fine scales associated with the complete breakup and violent mixing of the ejected fluid with the outer flow. The distortion of the fringes shows the strong vortical motions within the burst structure up to $y^+ \simeq 250$. It is not possible to assign a direction to the vortices since the pictures are two-dimensional and the object beam traversing the test section has an integrating effect in the spanwise direction. Also, the finest scales are obscured by the granular speckle inherent with

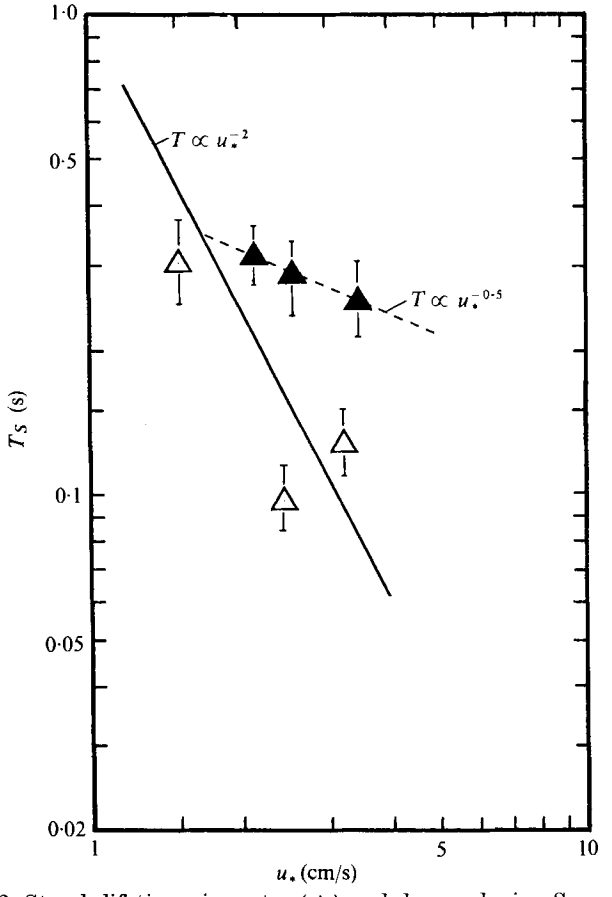

FIGURE 12. Streak lifetimes in water (△) and drag-reducing Separan (▲) flows.

laser light. The burst appears to be stretched outwards and away from the wall along a trajectory marked t in sketch 5. The ejected fluid is then convected downstream with the mean flow.

The effect of the drag-reducing polymer additive on the bursting process is shown in the frames of figure 10 (plate 4). The spatial scales and sketch markings conform to those already described for figure 9. There is an oscillatory growth of the fluid element as it bursts (frames 1–3, figure 10). However, the fluid element has a trajectory t more nearly parallel to the wall than in the case of water. A noticeable absence of the highly vortical small scale during burst breakup and reduced wall-normal extent ($y^+ \simeq 100$) of the ejected fluid are characteristic of the drag-reducing burst structure.

5.3. *Sublayer flow period.* The results of measurements of the burst rate F, burst time interval T_B and sublayer period T_S, defined in §4.4, are described here.

Burst frequency F and period T_B. Figure 11 shows the burst rate F, the number of bursts per second per cm of spanwise marking width, as a function of wall shear velocity for water and Separan flows. The water data approximate the formula $F \propto u_*^3$. The most noticeable feature is the large reduction of the burst rate in the Separan flows as compared with that in water flows.

The correlation of the time interval T_B between bursts and u_* is shown in both figure 12

and figure 14 (solid line). For both water and Separan, the values of T_B are distributed about the zero-pressure-gradient Newtonian line ($T_B \propto u_*^{-2}$), indicating that the time interval between bursts in water and in drag-reducing flows may be almost equal when the comparison is made at equal wall shears.

Streak lifetime T_S. T_B might be interpreted as the average lifetime of a streak (Kline *et al.* 1967). A more direct and $(F-\lambda)$-independent estimate T_S of the streak lifetime was obtained from autocorrelations of the concentration fluctuation from the plan view of wall-layer streaks (details in §4.4). The data in table 3 show that Separan at $u_* = 3{\cdot}45$ cm/s has a mean T_S about twice the value for water at $u_* = 3{\cdot}25$ cm/s. All the T_S data are shown in table 3 and on figure 12 (dotted line). The solid line on the same figure is for T_B data, shown for comparison with the T_S data points. A discussion of T_B and T_S data is provided in §6.2.

6. Discussion

6.1 *Comparison of results with data in literature*

Wall-layer streak spacing. The non-dimensional streak spacing λ^+ for the three water flows was found to be almost constant at a value of 87 ± 20 (figure 6). Since Kline and co-workers (1965, 1967) first obtained a mean value of $\lambda^+ \simeq 100$ in zero-pressure-gradient Newtonian wall layers, numerous experimenters have demonstrated the universal nature of this λ^+ value over various ranges of the parameters (Re, u_*, fluids and flow sections). In drag-reducing flows, the trends of three investigations of streak spacing (Fortuna & Hanratty 1972; Donohue *et al.* 1972; this work) show a modest to large increase in λ^+ with increasing drag reduction (figure 13). However, the functional form of the different sets of data appears to be affected by other parameters such as the type of polymer-solvent combination or the data analysis technique employed.

Fortuna & Hanratty (1972), who first hypothesized the increased streak spacing in drag-reducing flow, obtained the λ^+ value from a long-time-averaged spatial correlation of singals from an array of electrochemical probes mounted flush with the wall. The distance between zero crossings was used as a measure of $\frac{1}{2}\lambda$. However, very flat peaks of the correlation showed that long-time-averaging tends to smear out shorter-scale phenomena, thus making only the largest scales and most persistent streaks detectable. This aspect has been demonstrated by Gupta, Laufer & Kaplan (1971), who used an array of hot-wire anemometers in air to detect ordered spatial structures at a wall. Employing a variable-interval time-averaging technique, they have shown that spatial correlations gradually smear out as the averaging time is increased. Beyond a certain small value of the averaging time, no correlation was seen to exist.

Eckelman, Fortuna & Hanratty (1972) re-examined Fortuna's data by associating eddy patterns with spanwise variations of the instantaneous velocity gradient at the wall. These new estimates of λ^+, also shown in figure 13, appear to be more realistic. The results of Donohue *et al.* (1972) are direct visual measurements of dye-streak spacings from motion pictures, a frame of which can be considered as an almost instantaneous record of the flow pattern.

Although the measurements of Eckelman *et al.* (1972), Donohue *et al.* (1972) and this work use an almost uniform principle to obtain λ, i.e. instantaneous patterns or very short averaging times, there is no universal relation between λ^+ and the

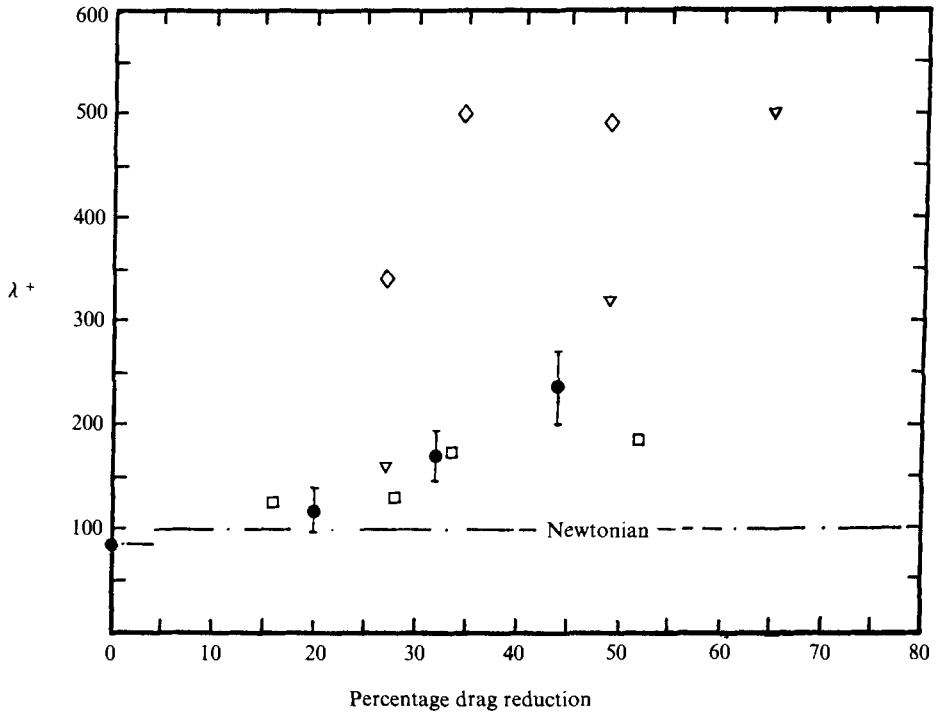

FIGURE 13. Non-dimensional streak spacing during drag reduction. ●, this work; □, Donohue *et al.* (1972); ▽, Eckelman *et al.* (1972); ◇, Fortuna & Hanratty (1972).

percentage drag reduction. This lack of correlation is possibly due to the effect of some polymer–solvent interaction, as yet unknown.

Bursting data. The solid line in figure 11 shows the burst rate for water to follow the functional form $F \propto u_*^3$, one similar to that found by Kline *et al.* (1967) in zero-pressure-gradient Newtonian channel flow. However, the line is shifted slightly, parallel to theirs and to lower values. An explanation for this shift of the data points may lie in the partial obscuring of bursts by each other during burst counting, a problem that gets worse with increasing u_*.

A noteworthy observation, suggested by Donohue *et al.* (1972) from their experiments, is that the time interval T_B between bursts computed from visual data for both Newtonian and drag-reducing flows is distributed about a single line given by the Kim–Kline–Reynolds model (see solid line in figure 14). Figure 14 correlates four decades of sublayer period, obtained from visual (T_B) and autocorrelation (T_S) measurements, and three decades of wall shear velocity u_*. Considering the different measurement techniques (see legend to figure 14), there is a noticeable tendency for all the Newtonian data to fall near the extended Kim–Kline–Reynolds line.

The significant trend of the drag-reducing T_S data (figures 12 and 14) is their departure from the Newtonian model for T_B. Autocorrelation measurements from this study for the streak lifetime T_S indicate a value in drag-reducing flows higher than the Newtonian value when the comparison is made at the same u_*. Partial support for this result comes from the work of Meek (1968) and Thomas & Greene (1973) and Thomas *et al.* (1973). Both Meek and Thomas made autocorrelation measurements at the

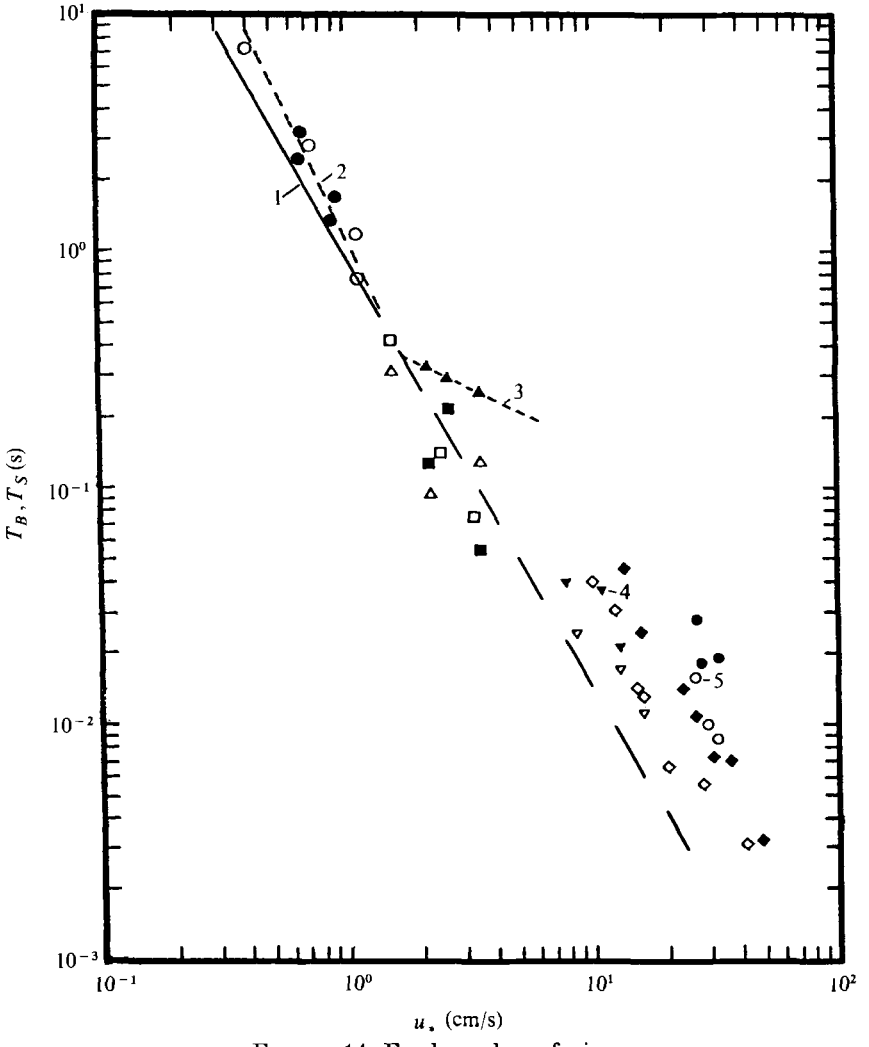

FIGURE 14. For legend see facing page.

pipe wall with hot-film anemometers. Although quantitative results for drag-reducing flows may be subject to some doubt owing to the use of hot-film probes, both workers found the sublayer period during drag reduction to be larger than the Newtonian value at the corresponding Reynolds number. Figure 14 shows their results recalculated on the basis of u_*.

6.2. *Comparison of T_S and T_B data*

The exact quantitative correspondence between T_S and T_B is not known. Qualitatively, they appear to be approximate estimates of the same quantity for Newtonian flow; i.e. the period of the wall-layer flow disturbance. The following aspects are readily seen on figure 12:

(i) T_S is approximately the same as T_B (solid line) for the three water flows;

(ii) T_S in drag-reducing Separan flow, i.e. $T_{S(DR)}$ is greater than the corresponding value for water, i.e. $T_{S(N)}$, when compared at approximately the same u_*;

(iii) $T_{S(DR)}$ is approximately proportional to $u_*^{-0.5}$, whereas $T_{S(N)} \approx T_{B(N)} \propto u_*^{-2}$. Some explanations are provided for the trends of the T_S and T_B data seen on figure 12.

Scanning the interferograms at a single point is analogous to having a single probe at that point in the flow. 'Streak lifetime' is then the length of time for which a streak (low-speed or high-speed zone) is continuously detectable at that point. However, a scanning point can fail to detect a particular streak passing that point in the following circumstances: (*a*) if that streak waves in the spanwise direction and out of line with the sampling point or (*b*) if that streak, being a low-speed zone, lifts up from the wall and disappears.

If it is assumed that the computed T_B is a correct estimate of the sublayer period in Newtonian flows, and if only circumstance (*b*) were effective in the determination of the autocorrelation, then the T_S estimate would be almost equal to T_B. However, streak waving [circumstance (*a*)] would tend to reduce the streak lifetime T_S as detected from $R_c(\tau)$, giving $T_S < T_B$. The data in figure 12 show $T_S < T_B$ for two of the three water runs. The difference between T_B and T_S for these water runs is small (see table 3). This

Description of figure 14

Figure 14. Sublayer-period data in Newtonian and drag-reducing flows.

No.	Reference	Experimental details	Data type
1	Kim *et al.* (1971)	—— Stanford data (1962–8) water, channel flow $T_B \propto u_*^{-2}$	[7] Visual‡ [2] Hot-wire auto-correlation§
2	Donohue *et al.* (1972)	○ Two-dimensional, D_H = 7·3 cm water	[8] Visual‡
		● 139 p.p.m. by weight Polyox-FRA	
		– – – corrected for pressure gradient	
3	This work	△ □ Pipe flow, D = 2·63 cm water	[6] Visual†
		▲ ■ 50 p.p.m. by weight Separan AP30	[6] Wall concentration autocorrelation§ Signal length/τ_l = 40*
		- - - - $T_S \propto u_*^{-0.5}$	
4	Thomas *et al.* (1973)	Pipe flow, D = 0·30 cm	
		▽ water	[6] Hot-film probe autocorrelations§ 10 < signal length/τ_l < 35
		▼ 20 p.p.m. by weight Separan AP30	
	Thomas & Greene (1973)	◇ 0·9 % by weight saline	
		◆ 40 p.p.m. by weight Separan AP273	[14] As above§ Signal length/τ_l > 1000
5	Meek (1968)	Pipe flow, D = 2·42 cm	
		○ tetralin	[6] Hot-film probe autocorrelations§
		● 200 p.p.m. by weight polyisobutylene in tetralin	

† Numbers in square brackets indicate data points available.
‡ T_B, time interval between bursts; computed as $1/F\lambda$.
§ T_S, streak lifetime; autocorrelation peak.
* τ_l = maximum lag time for autocorrelation.

may indicate that the apparent decrease in T_S below T_B owing to spanwise streak waving in the water flows is small, and that both T_S and T_B are good estimates of the sublayer flow period in Newtonian flow.

6.3. *Increased sublayer stability during drag reduction*

In the drag-reducing runs, $T_{S(DR)}$ exceeds $T_{S(N)}$ by a factor of 1·5–3. This trend is consistent with visual observations, which show greater streak persistence in the drag reducer as compared with water flow at the same u_*. Motion pictures of drag-reducing flows (Achia & Thompson 1974) give the impression that the solution is many times more viscous than water, although the solution's zero-shear-rate viscosity (ν_0 at $\dot{\tau} \to 0$) was only 0·0144 cm^2/s. This may be explained by the fact that dilute polymer solutions, when subjected to stretching actions, can exhibit a stretch-rate-dependent elongational viscosity ν_{el} (e.g. Metzner & Metzner 1970; Oliver & Bragg 1973). ν_{el} may have values many times larger than the viscosity as $\dot{\tau} \to 0$ and it makes the solution stretch resistant.

To identify the resistance to stretching of fluid bursts and streaks as a possible mechanism for drag reduction, the dominant wall-layer fluid motions and visual impressions are re-examined. The observed spanwise concentration distribution of the refractive-index enhancer provides a direct clue to the nature of spanwise stretching in the near-wall flow. The closely spaced sawtooth profile in the water flows and the more expanded profile in the drag reducer (see photographs in figure 7) suggest less spanwise stretching and compression in the latter. The lowered spanwise stretching in the drag reducer could be a direct result of an increase in the value of the solution's elongational viscosity $\nu_{el(DR)}$ over the Newtonian value $\nu_{el(N)}$. Thus the spanwise streak spacing, which increases above the Newtonian value during drag reduction, could be a measure of the change in ν_{el}.

In the calculation of λ^+_{DN} ($= \lambda u_*/\nu$) for the drag-reducing solution, ν_0 was used since ν_{el} was unknown. If the increased λ^+_{DR} during drag reduction (figure 6) were normalized to the constant Newtonian value λ^+_N, a measure of ν_{el} might be available. Thus the ratio $|\lambda^+_{DR}/\lambda^+_N|_{u_*}$ may give some measure of the factor by which ν_{el} in the drag-reducing flow is greater than the zero-shear-rate solution viscosity ν_0.

Assuming that λ^+_{DR} would have the same value as λ^+_N (an almost constant value for Newtonian wall layers) if the proper viscosity value were used in its calculation yields

$$\lambda^+_{DR} \equiv \lambda^+_N. \tag{17}$$

Expanding (17) gives

$$\lambda_{DR}\, u_{*(DR)}/\nu_{el(DR)} = \lambda_N\, u_{*(N)}/\nu_{el(N)}. \tag{18}$$

When a comparison is made at equal value of the wall shear, i.e. $u_{*(DR)} = u_{*(N)}$, (18) becomes

$$\nu_{el(DR)} = (\lambda_{DR}/\lambda_N)\, \nu_{el(N)}. \tag{19}$$

At the same u_*, $\lambda_{DR} > \lambda_N$. Also λ_{DR} increases with increasing u_* or increasing percentage drag reduction while λ_N decreases with increasing u_* (e.g. see figure 6). Equation (19) may be rewritten as

$$\frac{\nu_{el(DR)}}{\nu_{el(N)}} = \frac{\lambda^+_{DR}}{\lambda^+_N} \frac{\nu_{0(DR)}}{\nu_{0(N)}}, \tag{20}$$

Runs	Streak lifetime (s) $T_{S(DR)}$	Streak lifetime (s) $T_{S(N)}$ from line on figure 12	Streak spacing (non-dimensional) λ^+_{DR}	Streak spacing (non-dimensional) λ^+_N	$\left\lvert\frac{T_{S(DR)}}{T_{S(N)}}\right\rvert_{u_*}$	$\left\lvert\frac{\lambda^+_{DR}}{\lambda^+_N}\right\rvert_{u_*}$
*S*1	0·313	0·20	114	Constant	1·6	1·3
*S*2	0·285	0·150	170	mean	1·9	1·9
*S*3	0·255	0·080	235	$\simeq$ 87	3·2	2·7

TABLE 4. Ratios of streak lifetime and streak spacing.

when λ^+_{DR} is calculated for the drag-reducing solution on the basis of its $\dot{\tau} \to 0$ viscosity ν_0. In (20), $\nu_{el(N)}/\nu_{0(N)} = 3$, the Trouton ratio for a Newtonian fluid (Metzner 1968). Equation (20) becomes

$$\nu_{el(DR)}/\nu_{0(DR)} = 3\lambda^+_{DR}/\lambda^+_N. \tag{21}$$

Thus the ratio of the non-dimensional spanwise streak spacings could be a measure of the change in viscosity of the drag reducer owing to stretching motions. The ratio $3\lambda^+_{DR}/\lambda^+_N$ reflects the 'increased viscosity effect'.

In order to observe how the extensional viscosity might affect the wall-layer flow period, the ratios $|T_{S(DR)}/T_{S(N)}|_{u_*}$ and $|\lambda^+_{DR}/\lambda^+_N|_{u_*}$ were compared (see table 4). They are respectively the factors by which the streak lifetime and the non-dimensional streak spacing in the drag reducer are increased over the Newtonian value for the corresponding u_*. Inspection of the ratios indicates that

$$T_{S(DR)}/T_{S(N)} \simeq \lambda^+_{DR}/\lambda^+_N \tag{22}$$

at $u_{*(DR)} = u_{*(N)}$. This result is based on a limited set of data points that have an error range of about $\pm 15\,\%$ of the mean.

As an aside, it is interesting to note that, if the dashed line joining $T_{S(DR)}$ points in figure 12 is extrapolated back to the T_S Newtonian line, it intersects it at $u_* \simeq 1{\cdot}7$ cm/s. Gross flow data also show that the 'onset' of drag reduction occurs at $u_* \simeq 1{\cdot}7$ cm/s. The dashed line for $F \propto u_*^{1{\cdot}25}$ on figure 11 gives a similar onset u_*. It appears from figures 11 and 12 that for the drag-reducing flow F and $T_{S(DR)}$ depart gradually from the Newtonian line after onset. These observations suggest that the burst rate and streak lifetime in a drag-reducing flow may follow different proportionality laws relating them to u_* than they would in a Newtonian flow.

Stretching can also be postulated to occur during streak lift-up and the subsequent stages of bursting (see figures 9 and 10). Streak lift-up is probably triggered by large vortices in the mean flow (Offen & Kline 1974; Nychas, Hershey & Brodkey 1973) that 'draw out' bursts from the wall layer. This effect causes more rapid stretching than that caused by the spanwise stretching of streaks previously discussed, since fluid elements are moving away from the slower wall layers to the faster-moving bulk of the fluid. The direction of stretching may be oriented roughly along the burst trajectory t shown in figures 9 and 10. Bursts in water flows tend to lose their identity more rapidly than those in the drag-reducing flows. The intense shearing and stretching motions that lead to burst breakup appear to be inhibited in the drag reducer. The suppression of bursting could be due to the solution's resistance to stretching motions.

6.4. *The scales of eddy interactions*

The results of the visualization experiments are useful in re-examining the basis of space and time scales of turbulence that have been associated in the past with phenomenological models for drag-reducing flow (e.g. Astarita 1965; Hershey & Zakin 1967). In computing the Deborah number ($De = \theta/\Delta T$), it has been customary to use a theoretical 'fluid relaxation time' for θ and the inverse frequency of the small-scale dissipative eddies as a measure of the 'flow-imposed time' ΔT. Drag reduction is hypothesized to occur when $De \approx 1{\cdot}0$. θ and ΔT defined in the above-mentioned manner are subject to the following criticism.

The fluid relaxation time θ, estimated from the molecular theory of either Rouse & Sittel (1953) or Zimm (1956), has been assumed adequately to represent a drag-reducing solution's elastic property. θ has been calculated to be in the range 10^{-3} to 10^{-6} s (e.g. Hershey & Zakin 1967) for many dilute polymer solutions of interest in drag reduction. On the other hand, the recent measurements by Darby (1970) of the transient response characteristics of dilute Polyhall-295 solutions (100–500 p.p.m. by weight) have shown $\theta \simeq 0{\cdot}3$–$1{\cdot}4$ s for a shear-rate range of about 10–0·1 s^{-1}. These experimental θ values, although in the range of low shear rates, are probably more representative of the fluid time θ than those calculated from approximate molecular theories. Further, the theories predict a constant value of θ, which is contrary to the experimental result that θ decreases with increasing strain ($\theta \propto \gamma_{\max}^{-0{\cdot}4}$ from Darby 1970).

This leads to the question as to whether time-scale hypotheses have considered the proper spatial eddy scales of turbulence to arrive at ΔT, the characteristic 'flow time'. The visual results of this work and those of Donohue *et al.* (1972) indicate that the important scales in the wall layer of drag-reducing flows are those of the streaks and bursts. Bursts do not occur on the small 'dissipative' (Kolmogorov) scale; nor do they occur on large scales of the order of D. Instead, bursts may be considered as occurring on a medium-sized 'energy-containing' scale ($l \approx 0{\cdot}1$–$0{\cdot}4\ D$ in this study) that transports turbulent energy from the wall. It is the burst breakup process that gives rise to the small dissipative scales (e.g. see figure 9). Thus the characteristic 'flow time' may be properly represented by the time scales of the visualized wall-layer streaks and bursts.

For the elongational viscosity $\nu_{e(DR)}$ to be significantly larger than the zero-shear-rate value $\nu_{0(DR)}$, the duration of transient elongational flow must in general be of the same order of magnitude as θ (Denn & Marrucci 1971). A rough comparison of Darby's (1970) experimentally measured values of θ ($0{\cdot}3 < \theta < 1{\cdot}4$ s for $10 > \dot{\gamma} > 0{\cdot}1\ s^{-1}$) with the sublayer periods during drag reduction from the visualization experiments of this work ($0{\cdot}35 > T_B > 0{\cdot}06$ s; $2{\cdot}1 < u_* < 3{\cdot}6$ cm/s) and of Donohue *et al* (1972)

$$(3{\cdot}4 > T_B > 1{\cdot}3\,\text{s};\ 0{\cdot}6 < u_* < 0{\cdot}9\,\text{cm/s})$$

shows θ and the sublayer period to be of almost the same order of magnitude. The strain rates in the flow experiments ($6000 < Re < 18000$) could be an order of magnitude higher than those of Darby. However, the rate of decrease of θ with γ is very low, making this comparison valid.

Thus the use of the sublayer period as the characteristic 'flow time' and the length scale of the streak–burst structure as the length scale associated with this flow time

seems to be appropriate. It has been suggested (Donohue *et al.* 1972) that the characteristic 'fluid time' may be derived from a combination of ν_{el} and u_*. This choice of flow and fluid times appears to give the proper scales for describing drag-reducing flows.

The authors wish to acknowledge the support of this research by the National Research Council of Canada under grant A4936 and a special equipment grant for the argon laser. One of us (BUA) acknowledges the University of British Columbia for a Graduate Fellowship. Parts of this paper were presented at the British Hydromechanics Research Association Ist International Conference on Drag Reduction at Cambridge, England, in September 1974 and have been published in the conference proceedings (September 1975). Permission by BHRA to reproduce some of the material is acknowledged.

REFERENCES

ACHIA, B. U. 1972 *J. Phys.* E, *Sci. Instr.* **5**, 128.

ACHIA, B. U. 1975 Structure of pipe wall turbulence in Newtonian and drag-reducing flow: a hologram-interferometric study. Ph.D. thesis in Chemical Engineering, University of British Columbia (also M.A.Sc. thesis, 1971).

ACHIA, B. U. & THOMPSON, D. W. 1972 *Appl. Optics* **11**, 953.

ACHIA, B. U. & THOMPSON, D. W. 1974 *Int. Conf. Drag Reduction, Cambridge, England*, paper A2. Bedford: BHRA Fluid Engineering.

ARUNACHALAM, V. R., HUMMEL, R. L. & SMITH, J. W. 1972 *Can. J. Ch. E.* **50**, 337.

ASTARITA, G. 1965 *I & E.C. Fund.* **4**, 354.

CARPENTER, C. N. 1973 Drag reduction visual study. Ph.D. thesis, Ohio State University, Columbus.

CORINO, E. R. & BRODKEY, R. S. 1969 *J. Fluid Mech.* **37**, 1.

DARBY, R. 1970 *Trans. Soc. Rheol.* **14**, 185.

DENN, M. M. & MARRUCCI, G. 1971 *A.I.Ch.E. J.* **17**, 101.

DONOHUE, G. L. 1973 Hydrogen bubble flow visualization: limitations in drag-reducing polymer solutions. *Naval Undersea Center, San Diego, California, Release* no. 100.

DONOHUE, G. L., TIEDERMAN, W. G. & REISCHMAN, M. M. 1972 *J. Fluid Mech.* **56**, 559.

ECKELMAN, L. D., FORTUNA, G. & HANRATTY, T. J. 1972 *Nature Phys. Sci.* **236**, 94.

FORTUNA, G. & HANRATTY, T. J. 1972 *J. Fluid Mech.* **53**, 575.

GADD, G. E. 1965 *Nature* **206**, 463.

GUPTA, A. K., LAUFER, J. & KAPLAN, R. E. 1971 *J. Fluid Mech.* **50**, 493.

HERSHEY, H. C. & ZAKIN, J. L. 1967 *I. & E.C. Fund.* **6**, 381.

HOYT, J. W. 1972 *Trans. A.S.M.E., J. Basic Engng.* **94**, 258.

KIM, H. T., KLINE, S. J. & REYNOLDS, W. C. 1971 *J. Fluid Mech.* **50**, 133.

KLINE, S. J., REYNOLDS, W. C., SCHRAUB, F. A. & RUNSTADLER, P. W. 1967 *J. Fluid Mech.* **30**, 741.

LUMLEY, J. L. 1973 *J. Polymer Sci.: Macromol. Rev.* **7**, 263.

MEEK, R. L. 1968 A study of the viscous sublayer in turbulent flow. Ph.D. thesis, University of Utah, Salt Lake City.

METZNER, A. B. 1968 *Trans. A.S.M.E., J. Lub. Tech.* **90**, 531.

METZNER, A. B. & METZNER, A. P. 1970 *Rheologica Acta* **9**, 174.

NYCHAS, S. G., HERSHEY, H. C. & BRODKEY, R. S. 1973 *J. Fluid Mech.* **61**, 513.

OFFEN, G. R. & KLINE, S. J. 1974 *J. Fluid Mech.* **62**, 223.

OFFEN, G. R. & KLINE, S. J. 1975 *J. Fluid Mech.* **70**, 209.

OLIVER, D. R. & BRAGG, R. 1973 *Chem. Engng J.* **5**, 1.

ROLLIN, A. 1971 Similarity laws and turbulence structure of drag-reducing fluids. Ph.D. thesis, University of Alberta, Edmonton, Canada.

ROUSE, P. E. & Sittel, K. 1953 *J. Appl. Phys.* **24**, 690.

RUDD, M. J. 1972 *J. Fluid Mech.* **51**, 673.

SCHRAUB, F. A. & KLINE, S. J. 1965 A study of the structure of the turbulent boundary layer with and without longitudinal pressure gradients, *Dept. Mech. Engng, Stanford Univ., California, Rep.* MD–12.

SEYER, F. A. & METZNER, A. B. 1969 *A.I.Ch.E. J.* **15**, 426.

THOMAS, L. C. & GREENE, H. L. 1973 *Proc. Symp. Turbulence in Liquids, Univ. Missouri, Rolla* (ed. G. K. Patterson & J. L. Zakin), p. 394.

THOMAS, L. C., GREENE, H. L., NOKES, R. F. & CHU, M. 1973 *A.I.Ch.E. Symp. Ser.* **130**, 14.

WELLS, C. S. & SPANGLER, J. G. 1967 *Phys. Fluids* **10**, 1890.

ZIMM, B. H. 1956 *J. Chem. Phys.* **24**, 264.

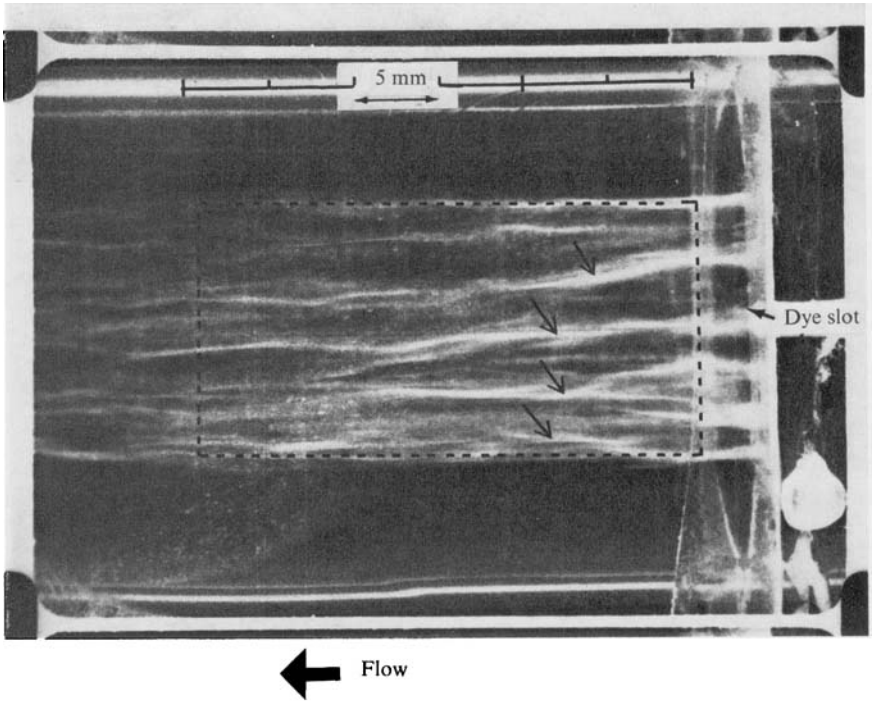

(*a*)

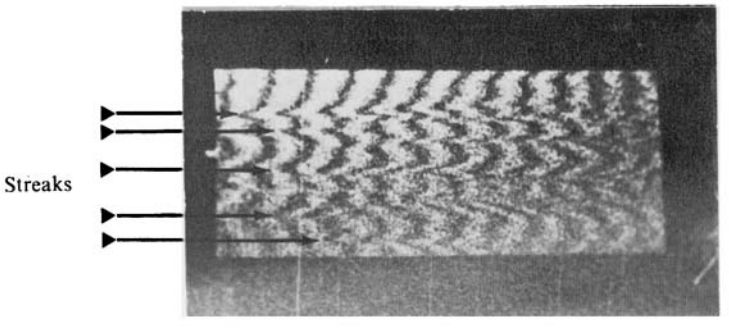

(*b*)

FIGURE 3. Streaks at the pipe wall in turbulent flow. (*a*) As visualized by wall-slot dye injection. (*b*) As seen through a hologram with a refractive-index enhancer infused at the wall. (The dotted line on (*a*) is the framed region in (*b*).)

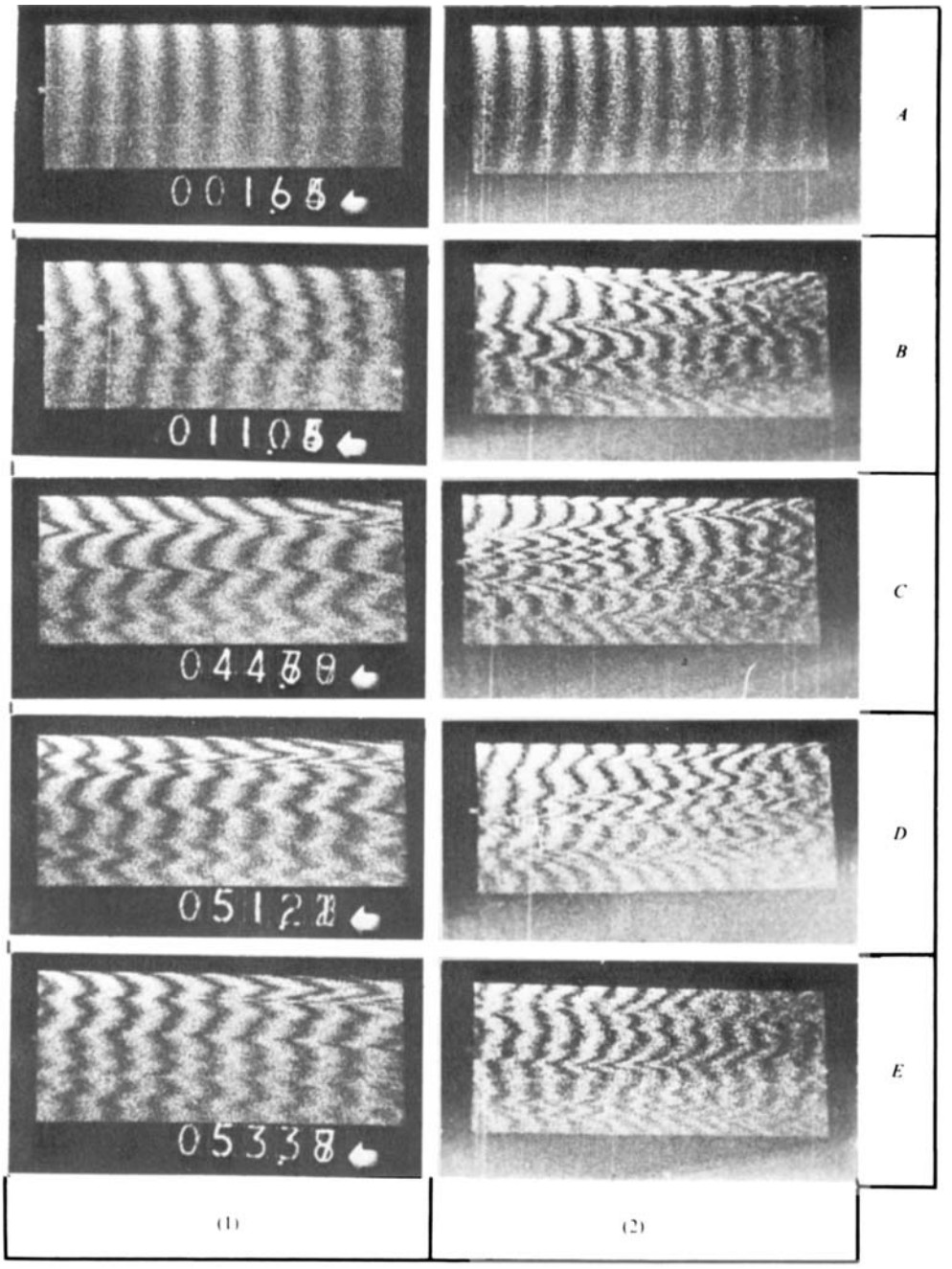

FIGURE 7. Real-time flow interferograms showing the variation in spanwise concentration at the pipe wall in (1) Separan ($u_* = 3{\cdot}45$ cm/s) and (2) water ($u_* = 3{\cdot}25$ cm/s). (The spatial scale is same as for figure 3.)

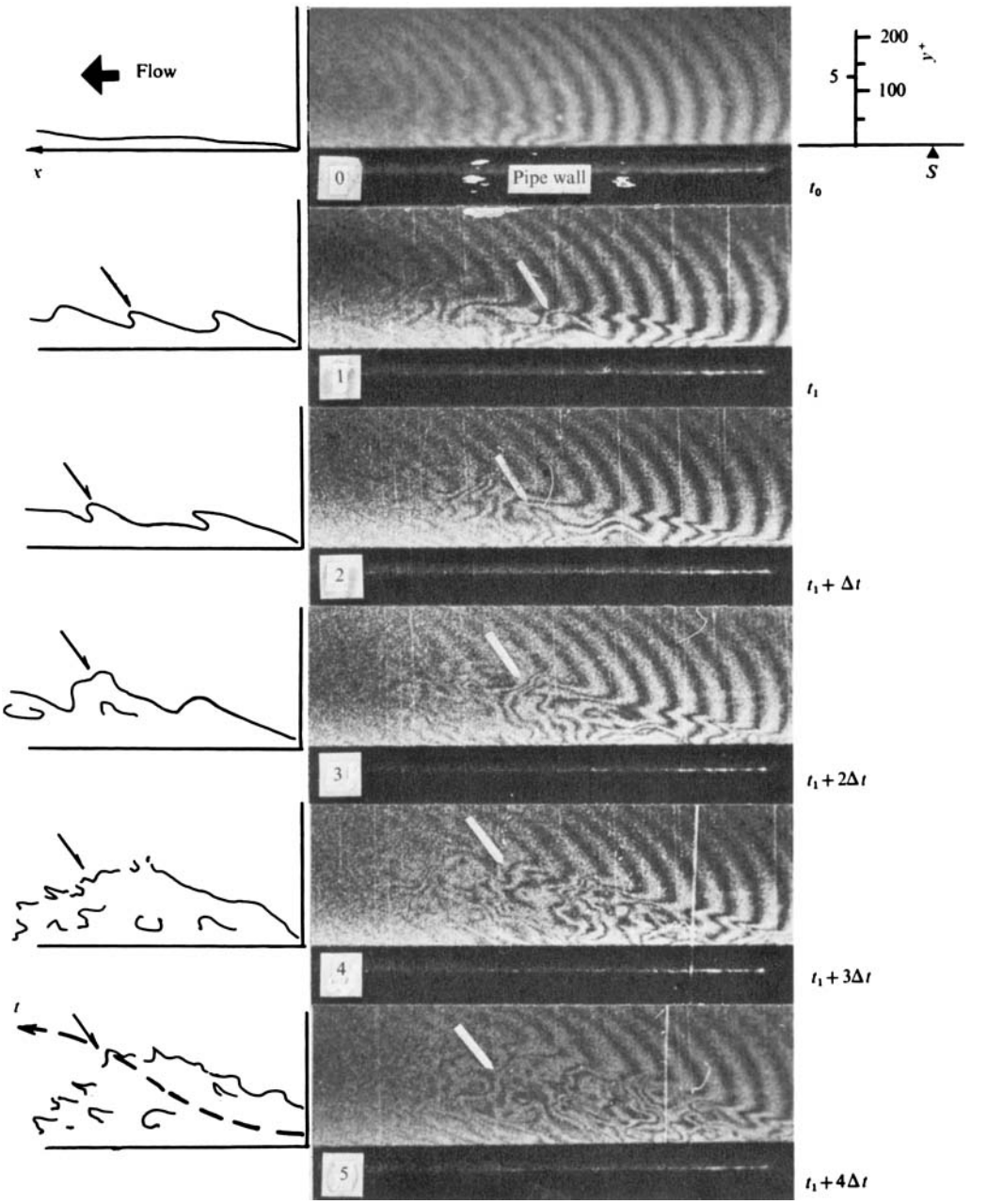

FIGURE 9. Bursting sequence in a water flow. $u_* = 2{\cdot}45$ cm/s; y^+ at 100 $\simeq$ 0·40 cm. S indicates the location of the wall slot. $\Delta t = 0{\cdot}016$s.

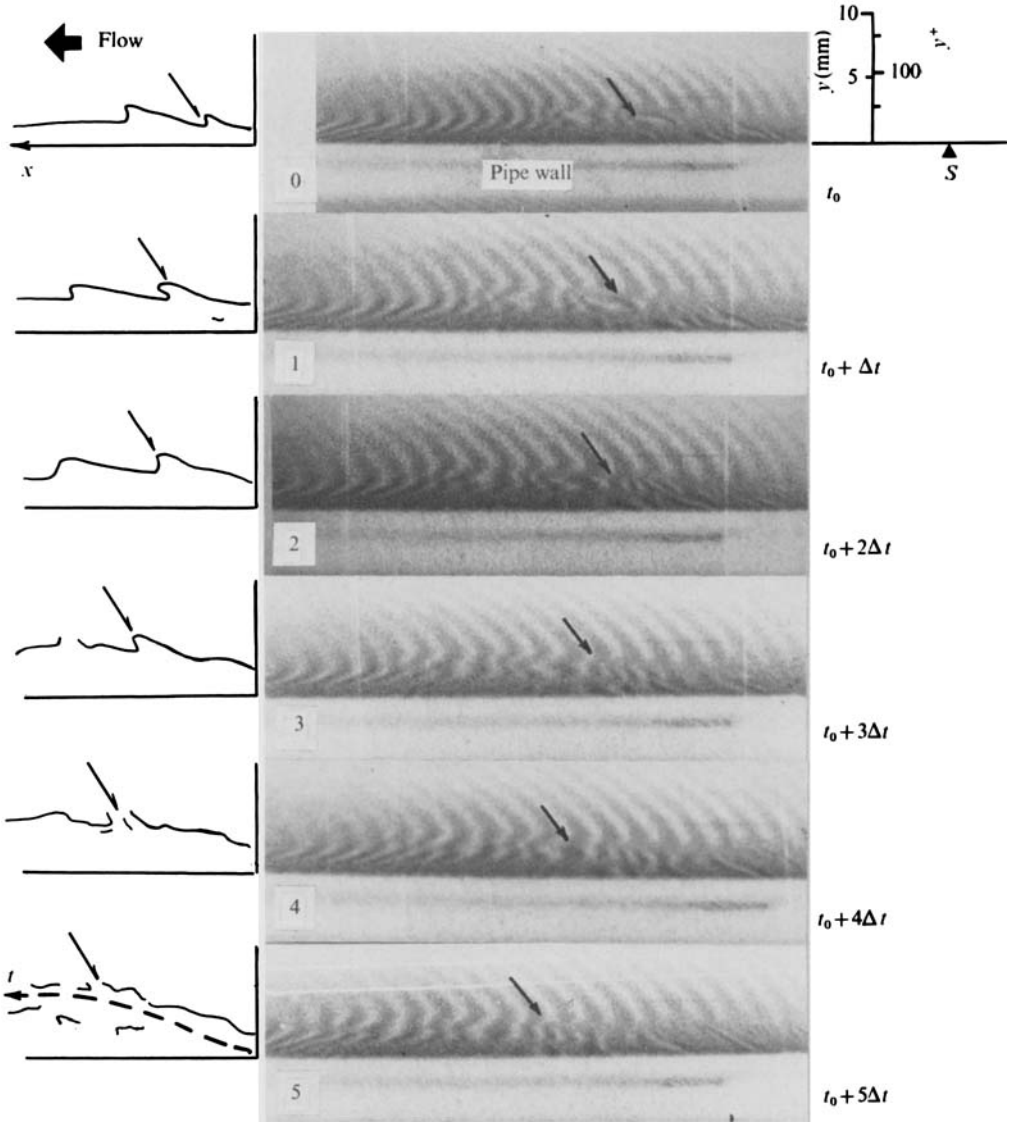

FIGURE 10. Bursting sequence in a drag-reducing Separan flow. $u_* = 2{\cdot}56$ cm/s; y^+ at $100 \simeq 0{\cdot}55$ cm. S indicates the location of the wall slot. $\Delta t = 0{\cdot}016$s.